Arab J Sci Eng (2017) 42:4759–4769
DOI 10.1007/s13369-017-2649-1

RESEARCH ARTICLE - MECHANICAL ENGINEERING

A Comparative Study on Mode I and Mode II Interlaminar Behavior of Borax and SiC Particles Toughened S-Glass Fabric/Epoxy Composite

Mohamad Alsaadi[1,2] · **Ahmet Erkliğ**[2]

Received: 10 November 2016 / Accepted: 7 June 2017 / Published online: 16 June 2017
© King Fahd University of Petroleum & Minerals 2017

Abstract The aim of this manuscript is to study experimentally the mechanical properties and interlaminar fracture toughness for mode I and mode II delamination of borax and silicon carbide particles- modified S-glass fiber-reinforced epoxy (GFRE) composites. Composite specimens were prepared and tested according to ASTM standards with borax and silicon carbide particle contents of 5, 10, 15 and 20% of the total resin weight. The reason for properties enhancement was explained based on scanning electron microscopy. The results indicated that the tensile strength and flexural strength reached maximum with increment of 10.5 and 51%, respectively, at borax content of 10 wt%, compared to 1.5 and 24.2% with silicon carbide content of 10 and 5 wt%, respectively. Mode I and mode II interlaminar fracture toughness were optimum at borax content of 15 and 10 wt%, with increment of 45.8 and 27.6%, respectively, compared to 36.7 and 46.5% at SiC particles of 10 and 5 wt%, respectively. Due to lower cost and good interlaminar fracture and mechanical properties of the borax–GFRE composites, borax can be used as particulate filler within fiber- reinforced polymer composites.

Keywords Borax · Glass fiber · Epoxy · Fracture toughness · Delamination

✉ Mohamad Alsaadi
phd.mohamadalsaadi@gmail.com;
mohamad.alsaadi@mail2.gantep.edu.tr

[1] Materials Engineering Department, University of Technology, Baghdad 10066, Iraq

[2] Mechanical Engineering Department, Faculty of Engineering, Gaziantep University, 27310 Gaziantep, Turkey

1 Introduction

Glass fibers-reinforced polymer (GFRP) composites have superior properties such as high stiffness, strength, thermal stability and resistance to chemical hurt [1]. However, GFRP is often limited from using in automobile, medical applications, aviation, construction and military application due to poor resistance to interlaminar fracture [2,3]. This issue may be ascribed to the lack of fibers reinforcement oriented in the laminate depth for effective transverse of the applied force that can be circumvented by Z-fiber stitching or pinning other fibers to join layers [4–6]. However, tensile properties of composites reduce by this technique and need others manufacturing procedures [7]. Therefore, the most polymer that has been usually used in these laminates is epoxy. To date, two procedures have been used to improve interlaminar fracture toughness. First, researchers have used special structures of epoxy, like dendritic hyperbranched polymers; nevertheless, the interlaminar fracture resistance needs more improving [8]. The other method, epoxy matrix, is toughened by incorporating additional constituents, thermoplastics [9] and rubber particles [10]. For thermoplastics, epoxy viscosity is extremely elevated after high molecular weight thermoplastics are mixed with the epoxy resin, which causes difficulties in composite laminate fabrication. In rubber particles, the same as thermoplastic do, even though the interlaminar fracture toughness is usually elevated due to the phase-separated structure in blends, the modulus and strength are dropped.

In recent years, particular attention has been paid to the rigid inorganic particulate fillers, especially nanoparticles like nano-clay, nano-silica, carbon nanotubes and nano-alumina [11–20], due to their improvement for interlaminar fracture toughness of fiber-reinforced epoxy resin in composites. Hsieh and Huang [21] prepared carbon fiber-

reinforced epoxy composites filled with aerogels particles (its carbon structure had a purity of 99.9%). The results showed that modulus, strength and delamination fracture energy of the laminates were increased by the addition of the aerogel to the composite laminates. Wang et al. [22] used Al_2O_3 microparticles to raise flexural strength, impact strength and mode II interlaminar toughness by 16, 37 and 50.0%, respectively, for carbon fiber-reinforced epoxy composite. Chisholm et al. [23] showed that the inclusion of SiC micro- and nanoparticles to carbon fabric/epoxy composite improved the tensile and flexural strength and modulus. Therefore, compared with the previously stated methods, the inclusion of particles can enhance mechanical properties and delamination fracture energy. Thus, it is more appropriate to study the effects of micro- and nanoparticle content, especially cheap particulate filler like borax, on the property and mechanism of interlaminar fracture toughness to be more clarified.

Borax is boron based available as a powder or granular form fire retardants that commonly used in polymers, wood products as flame retardant. Large quantities of borax can be harmful to plants and animals. Boron compounds have been noticeably used since 1980s in terms of being non-toxic and high biological, chemical and thermal resistance [24–27]. Cavdar et al. [28] produced composite laminates by adding borax, boric and wood flour in polyethylene (HDPE) matrix, in which the tensile and flexural modulus increased by 19 and 57%, respectively, at 40 wt% borax/wood flour-reinforced HDPE. Ayrilmis et al. [29] found that epoxy resin with mixture contents 2, 4 and 8 wt% of borax/boric (1:1 by weight) causes improvement in tensile strength, tensile modulus, impact strength and some physical properties such as water resistance. Gumus et al. [30] investigated several parameters affecting the electrorheological properties such as volume fraction, shear stress, frequency, temperature and electric field strength of the borax-modified polythiophene matrix composite. The results showed that the shear stress increased with the addition of borax up to 25% of volume fraction, and creep-recovery and vibration damping characteristics were also enhanced.

Based on the literature, many studies have been examined the influence of micro- and nanoparticles on the mechanical properties and interlaminar fracture toughness of fiber-reinforced polymer (FRP) composite. However, researchers in the literature did not investigate the effect of borax particle content on the interlaminar fracture toughness of FRP composite. The focus of this study is to examine the effect of borax (Bx) and silicon carbide (SiC) particle content on the tensile strength, flexural properties and interlaminar fracture toughness of mode I and mode II deformation of GFRE composite. The forms of failure and deformation were investigated using scanning electron microscopy.

2 Materials and Methods

2.1 Materials

The laminate composites were fabricated using epoxy (MOMENTIVE-MGS L285) and hardener (MOMENTIVE-MGS H285) in a stoichiometric ratio of 100/40,woven plain S-glass fabric layers with areal density of 200 g/m^2. The epoxy, hardener and S-glass fiber are provided by DOST Chemical Industrial Raw Materials Industry, Turkey. Borax (99% sodium tetraborate decahydrate) was supplied by Eti Mine Works General Management, Turkey. The chemical formula of the dry borax is ($Na_2B_4O_7$). It is composed of boric oxide (B_2O_3) and sodium oxide (Na_2O). The SiC particles were supplied by Eti Mine Works General Management, Turkey.

2.2 Composites Production and Samples Preparation

The borax and SiC particles in the range of 1–35 μm and 35 μm with bulk density of 0.52 and 1.49 gr/cm^3, respectively, were used in this study with four particle contents of 5, 10, 15 and 20 wt%. The composite laminates were produced by adding borax or SiC particles in epoxy resin. To obtain a homogeneous particulate resin, the measured quantity of particles was mixed with epoxy by a mechanical stirrer for 27 min with a constant speed of 755 RPM. Then, hardener was added to the particulate epoxy for quick setting. The resin mixture was applied to the fabric layers layer by layer at room temperature 25 °C. To make a starter crack for double-cantilever beam (DCB) and end-notched flexure (ENF) specimens, a heat-resistant Teflon film with thickness of 12 μm was inserted at the mid plane of the laminate during hand layup process. Then, laminated fabrics were subjected to 0.3 MPa pressure for 1 h curing time with 80 °C temperature (production process and unit are shown in Fig. 1). Afterward, laminate with size of 230 mm × 290 mm was cooled to the room temperature under the pressure. Then, composite laminates were cut according to ASTM standards using CNC machine to produce the tensile, flexural, DCB and ENF specimens.

2.3 Tensile and Flexural Specimens Test

The Shimadzu testing machine AG-X series (Kyoto, Japan) were used to test the tensile, flexural, DCB and ENF specimens. The specimens' thickness was in range of 3.4 ± 0.4 mm. At least three specimens were tested for each GFRE composite, borax particle-filled glass/epoxy (Bx-GFRE) and SiC particle-filled glass/epoxy (SiC-GFRE) composite that average values of the results were calculated. The specimens of tensile and flexural test were prepared in accordance with ASTM D 638 in size of 165 × 13 mm for a gauge length of

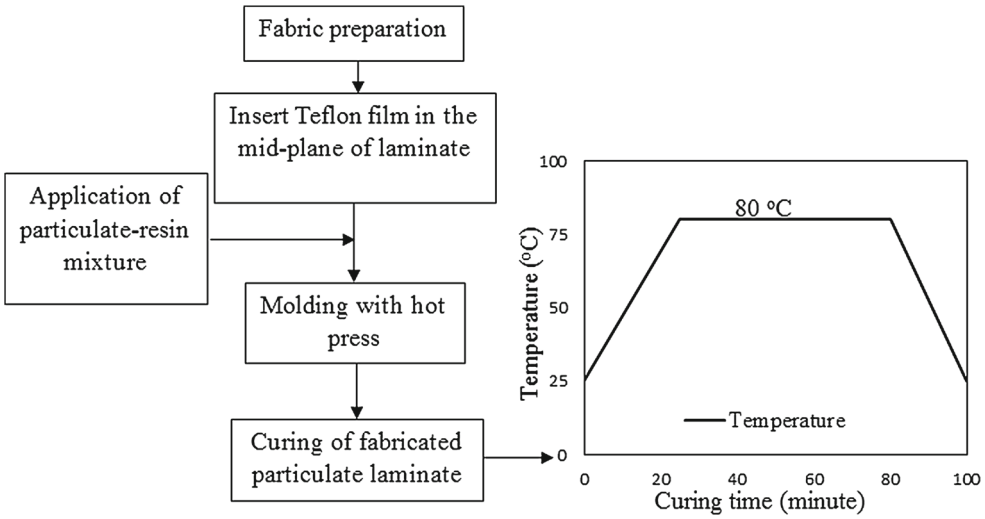

Fig. 1 Production process and unit

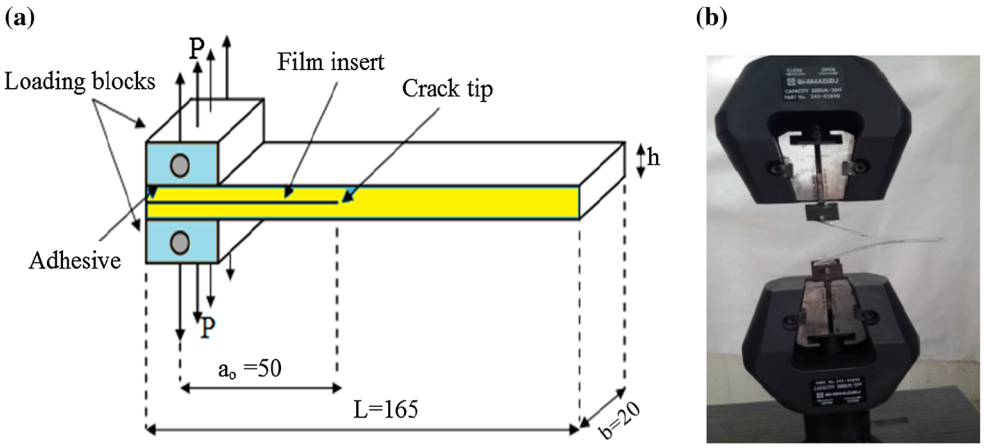

Fig. 2 **a** Configuration of the DCB test specimen, **b** DCB specimen under testing

50 mm and ASTM D 790 in size of 185 × 12.7 mm with span to thickness ratio of 32:1, respectively. The crosshead speeds for tensile and flexural testing were 2 and 4 mm/min, respectively.

2.4 DCB Specimens Test

The mode I delamination energy (G_{IC}) of the GFRE, Bx-GFRE and SiC-GFRE composite specimens was calculated using the DCB tests according to the ASTM D 5528 standard [31]. The DCB specimens were prepared with size of 165 × 20 mm. The aluminum loading blocks with size of 20 × 25 × 12 mm with a loading hole of 6 mm diameter were stuck to the each side on the cracked end of the specimen using adhesive Araldite 2014. The pre-crack length (a_o) according to the inserted film was 50 mm. The configuration of DCB test specimen and a picture for specimen during testing are presented in Fig. 2. The crosshead displacement of the DCB test was explained as crack opening displacement (COD) of the specimen. The crack propagation length was recorded using a digital camera. The crosshead speed of DCB tests was 5 mm/min according to ASTM D 5528. The data of DCB test were recorded in terms of P-COD and corresponding P-a values, which refer to crack extension length. The general formula from linear elastic fracture mechanics is used to evaluate G_{IC} as follows [2]:

$$G_{IC} = \frac{P^2}{2b}\frac{\partial C}{\partial a} = \frac{P\delta}{2bC}\frac{\partial C}{\partial a} \quad (1)$$

where P is the load applied at which the crack grows, b is the specimen width, a is the crack length, δ is the COD and C is the compliance equal to δ/P. Indeed, the DCB is not perfectly built-in; therefore, corrections are needed due to rotation and deformation around the crack tip. The crack length can be modified with a slightly longer $a + |\Delta|$, where

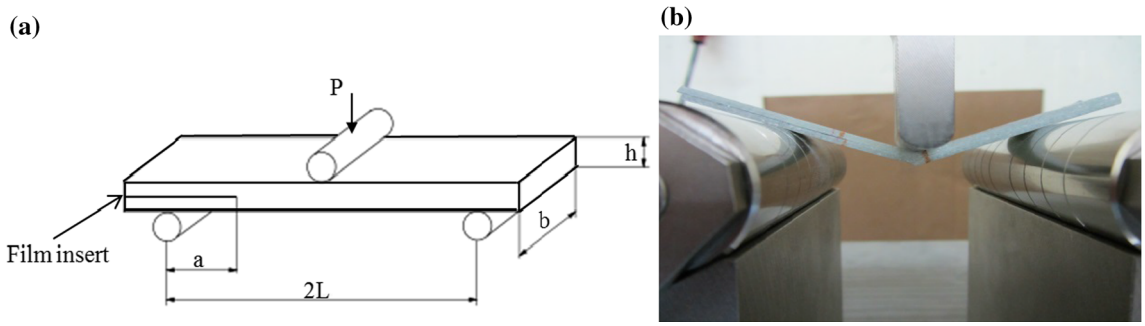

Fig. 3 **a** Dimensions of the ENF specimen, **b** ENF specimen under testing

Table 1 Mechanical properties of the composites

Composite type	Filler content (wt%)	Tensile strength (MPa)	Flexural strength (MPa)	Flexural modulus (MPa)
GFRE	0	389 (±9)	410 (±11)	21.0 (±0.32)
Bx_5-GFRE	5	418 (±17)	574 (±21)	23.5 (±0.75)
Bx_{10}-GFRE	10	430 (±11)	619 (±15)	24.5 (±0.94)
Bx_{15}-GFRE	15	401 (±13)	571 (±19)	22.3 (±0.58)
Bx_{20}-GFRE	20	394 (±15)	491 (±17)	21.2 (±0.40)
SiC_5-GFRE	5	374 (±12)	422 (±15)	19.3 (±0.40)
SiC_{10}-GFRE	10	395 (±17)	440 (±7)	18.7 (±0.09)
SiC_{15}-GFRE	15	354 (±9)	509 (±16)	19.6 (±0.20)
SiC_{20}-GFRE	20	344 (±11)	476 (±24)	18.1 (±0.75)

Δ can be determined by plotting cube root of the compliance, $C^{1/3}$ with respect to the crack extension length. After differentiating and substitution into equations 1, the mode I fracture toughness becomes [2,31,32]:

$$G_{IC} = \frac{3P\delta}{2b\,(a + |\Delta|)} \tag{2}$$

2.5 ENF Specimens Test

To determine the mode II delamination energy (G_{IIC}), the ENF tests were conducted on composite specimens. The three-point bending loading was applied to the specimens (Fig. 3) with a span length of 76 mm [36]. The ENF specimens were fabricated with size of 120 × 20 mm, and (a/L) was 0.5 at the crack propagation. Controlling displacement was used with a loading rate of 1 mm/min [33,34]. The ENF specimens create shear stress at the crack tip during the test. Therefore, the load suddenly decreased when the crack propagation starts and the specimen failed. To evaluate G_{IIC}, the direct beam theory was adopted as [33–37]:

$$G_{IIC} = \frac{9P\delta a^2}{2b\left(2L^3 + 3a^3\right)} \tag{3}$$

3 Results and Discussion

3.1 Effect of Particle Content on Mechanical Properties

Tensile and flexural strength and flexural modulus of GFRE, Bx-GFRE and SiC-GFRE composites are given in Table 1; also tensile and flexural strength results are shown in Fig. 4. As illustrated in Fig. 4, the tensile strength is 430 and 395 MPa at Bx and SiC content of 10 wt% with highest increment of 10.5 and 1.5%, respectively, compared to tensile strength of GFRE composite. Hence, the composite tensile strength regularly improved with adding borax up to 10 wt% and then followed the trend of decreasing to reach 394 MPa at 20 wt% of borax. The same behavior was observed for the flexural strength versus Bx and SiC particle content. The highest improvement of flexural strength was obtained at Bx and SiC particle content of 10 and 15 wt% with highest increment of 51 and 24.2%, respectively. In general, all the specimens of the Bx-GFRE and SiC-GFRE composites have flexural strength higher than GFRE composite. For example, the flexural strength for Bx-GFRE specimens increased from 410 to 619 MPa when the borax content changed from 0 to 10 wt%; then, further increasing borax particles, the flexural strength reduced to 491 MPa.

Furthermore, the flexural modulus of Bx-GFRE and SiC-GFRE composites (Table 1) was affected by the inclusion of

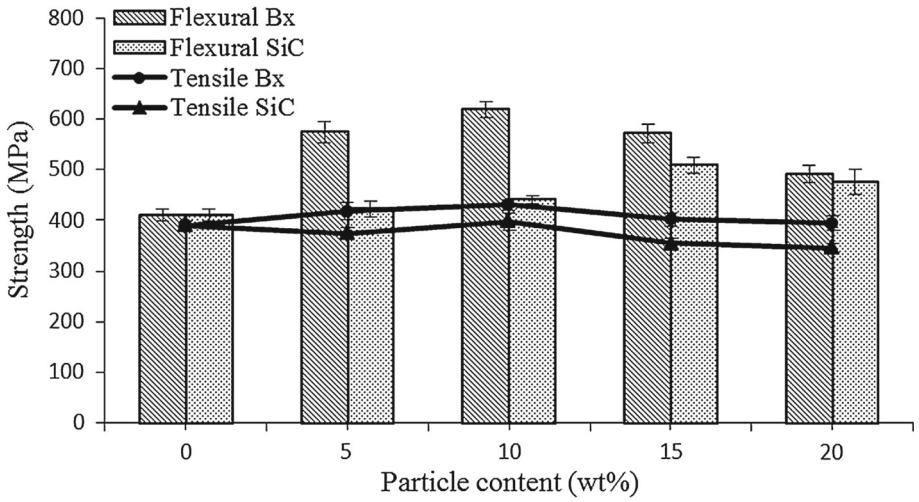

Fig. 4 Tensile and flexural strength versus particle content for the GFRE, Bx-GFRE and SiC-GFRE composites

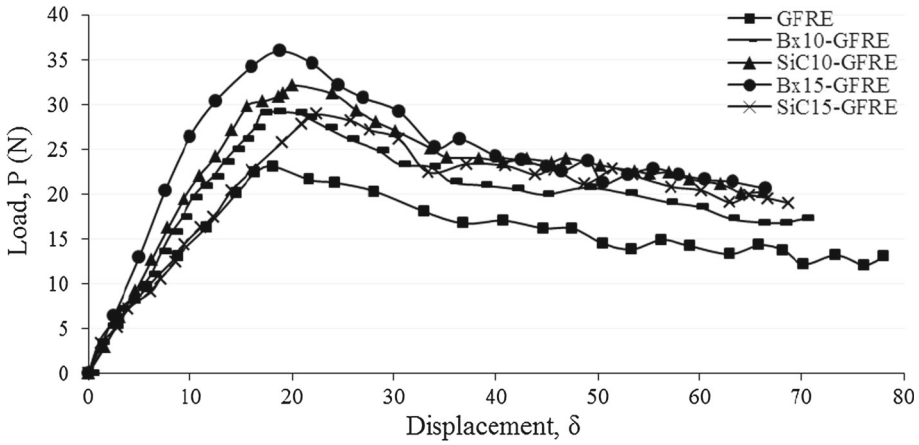

Fig. 5 Load–COD curves for the GFRE, Bx-GFRE and SiC-GFRE composites

Bx and SiC particles that the modulus improved by 16.7% at borax content of 10 wt%. Whereas the flexural modulus was degraded with the addition of SiC particles, this strategy of using cheap industrial inorganic particles like borax at least partly enhanced the mechanical properties.

As a result of the tensile and flexural experiments, the incorporation of borax particles within GFRE composite actually remarkably improved the flexural properties and tensile strength. The drop of the strength values may be attributed to the particle aggregation when the borax content more than 10 wt%, forming weaknesses in the composite.

3.2 Effect of Particle Content on Mode I Delamination Energy

The load–COD curves obtained by conducting DCB tests on specimens of GFRE composite toughened by Bx and SiC particles with contents of 10 and 15 wt% are shown in Fig. 5. This figure indicates that the GFRE, Bx-GFRE and SiC-GFRE composites exhibit a linear load–COD behavior up to the crack initiation point, then these curves exhibit nonlinear crack growth behavior. Furthermore, the gap was small between the nonlinear point and highest load point. In addition, the maximum load increased by the addition of Bx and SiC. The optimum load values occurred at 10 wt% of Bx and 15 wt% of SiC. The highest load–COD of GFRE was about 23 N–78 mm, while that of Bx-GFRE composites was about 28 N–76 mm, 29 N–70 mm, 36 N–70 mm and 33 N–68 mm, respectively, when the borax content was changed from 5, 10, 15 to 20 wt%, as presented in Table 2.

Indeed, the fracture onset means the highest load–COD value, which represents the converting from the linear to nonlinear behavior in the load–COD curve. In the delamination extension, the bridged fibers were cracked or peel off from the epoxy matrix and the separation of the both sides of the specimen increased, in which this behavior explains that propagation fracture toughness (G_{IC}-Prop) higher than initiation fracture toughness (G_{IC}-Onset) [38–40].

Figure 6 illustrates R-curves for the composite systems. These curves demonstrate the variation of G_{IC} versus delamination length of the GFRE, Bx-GFRE and SiC-GFRE composites. The values of G_{IC}-Onset and G_{IC}-Prop were defined according to the ASTM D-5528 standards [32] G_{IC}-Onset at the highest load point and G_{IC}-Prop corresponding

Table 2 Mode I delamination properties of the composites

Composite type	Filler content (wt%)	Highest load (N)	Highest COD (mm)	G_{IC}-Onest (J/m^2)	G_{IC}-Onest increment (%)	G_{IC}-Prop (J/m^2)	G_{IC}-Prop increment (%)
GFRE	0	23.3 (±1.7)	78.1 (±3.9)	441 (±18)	–	615 (±27)	–
Bx_5-GFRE	5	27.9 (±1.4)	76.4 (±2.1)	453 (±22)	2.8	645 (±32)	4.9
Bx_{10}-GFRE	10	29.2 (±1.0)	70.3 (±3.3)	558 (±13)	26.6	691 (±25)	12.4
Bx_{15}-GFRE	15	35.5 (±2.2)	69.6 (±3.4)	667 (±26)	45.8	823 (±33)	33.8
Bx_{20}-GFRE	20	32.8 (±1.3)	67.5 (±2.5)	570 (±27)	29.3	749 (±26)	26.9
SiC_5-GFRE	5	29.3 (±1.8)	68.4 (±2.8)	54 (±34)	22.9	663 (±25)	7.8
SiC_{10}-GFRE	10	32.1 (±1.9)	66.2 (±2.3)	603 (±40)	36.7	783 (±32)	27.3
SiC_{15}-GFRE	15	28.8 (±1.6)	68.7 (±3.2)	58 (±32)	32.7	705 (±42)	9.1
SiC_{20}-GFRE	20	30.9 (±1.8)	70.1 (±2.6)	475 (±25)	7.7	671 (±35)	14.6

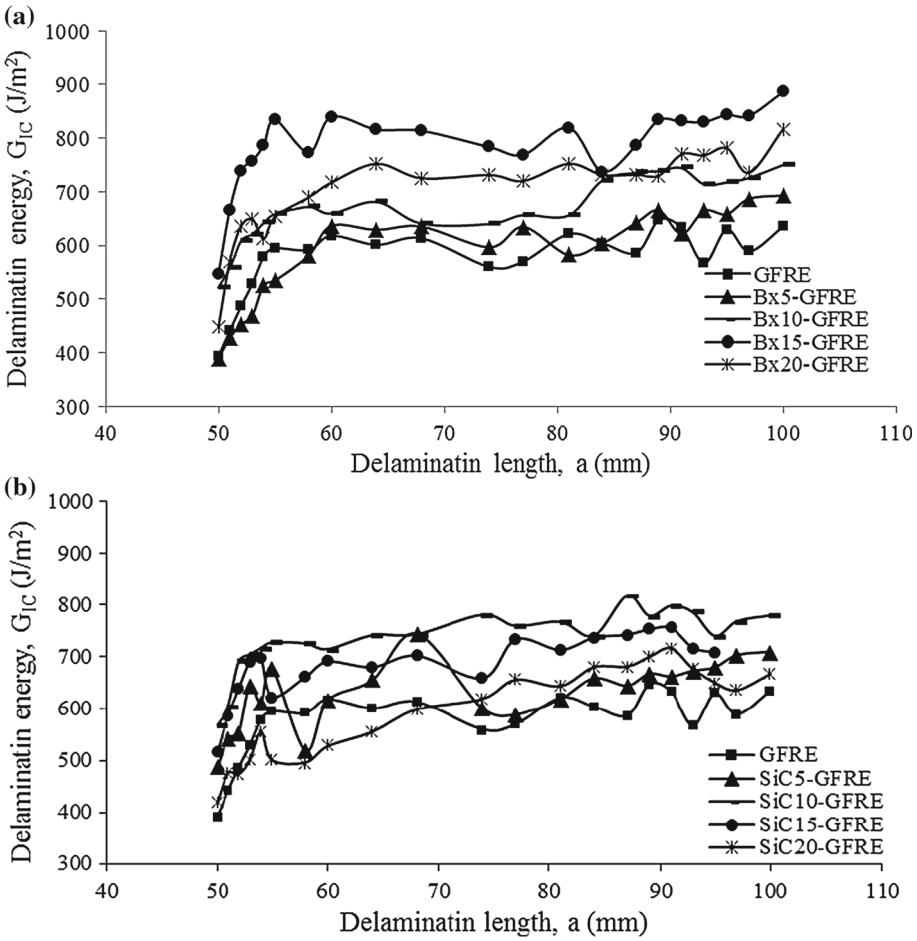

Fig. 6 R-curves for the **a** Bx-GFRE and **b** SiC-GFRE composites

to the average propagation values after highest G_{IC} value of the R-curves.

As shown in Fig. 7, G_{IC}-Onset and G_{IC}-Prop are improved with the addition of Bx more than addition of SiC in GFRE laminate. Hence, the G_{IC}-Onset of GFRE composite was 441 J/m^2. When the borax content increased from 5 to 15 wt%, the G_{IC}-Onset increased from 453 to 667 J/m^2 and then decreased to 570 J/m^2 at particle content of 20 wt%. Therefore, the G_{IC}-Onset increased by 2.8, 26.6, 45.8 and 29.3%, respectively, compared with GFRE composite. While with SiC addition, the highest increment of G_{IC}-Onset was 36.7% at SiC content of 10 wt%. The G_{IC}-Prop of GFRE composite was 615 J/m^2. When the borax content increased from 5 to 15 wt%, the G_{IC}-Prop increased from 645 to 823 J/m^2 and then decreased to 749 J/m^2 at borax content of 20 wt%. The G_{IC}-Prop increased by 4.9, 12.4, 33.8 and 26.9%, respec-

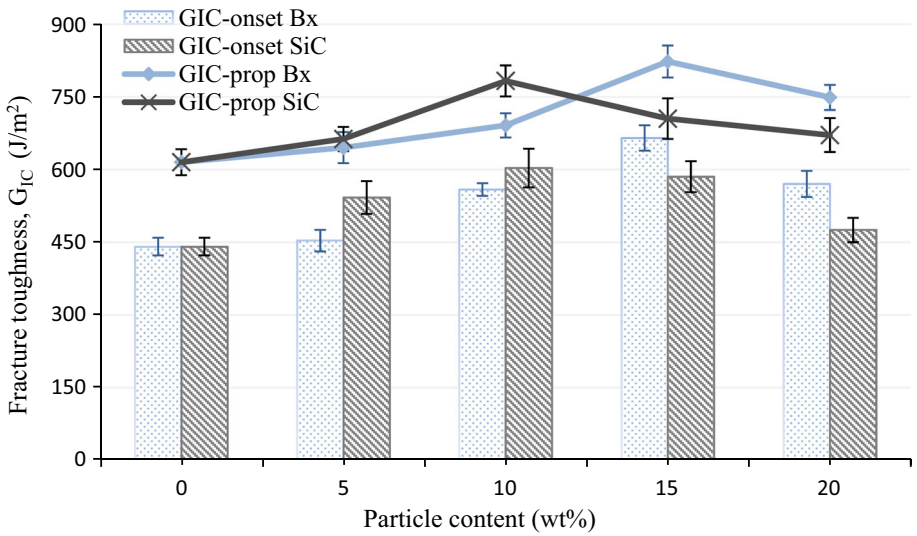

Fig. 7 Comparison of mode I fracture toughness among GFRE, Bx-GFRE and SiC-GFRE composites

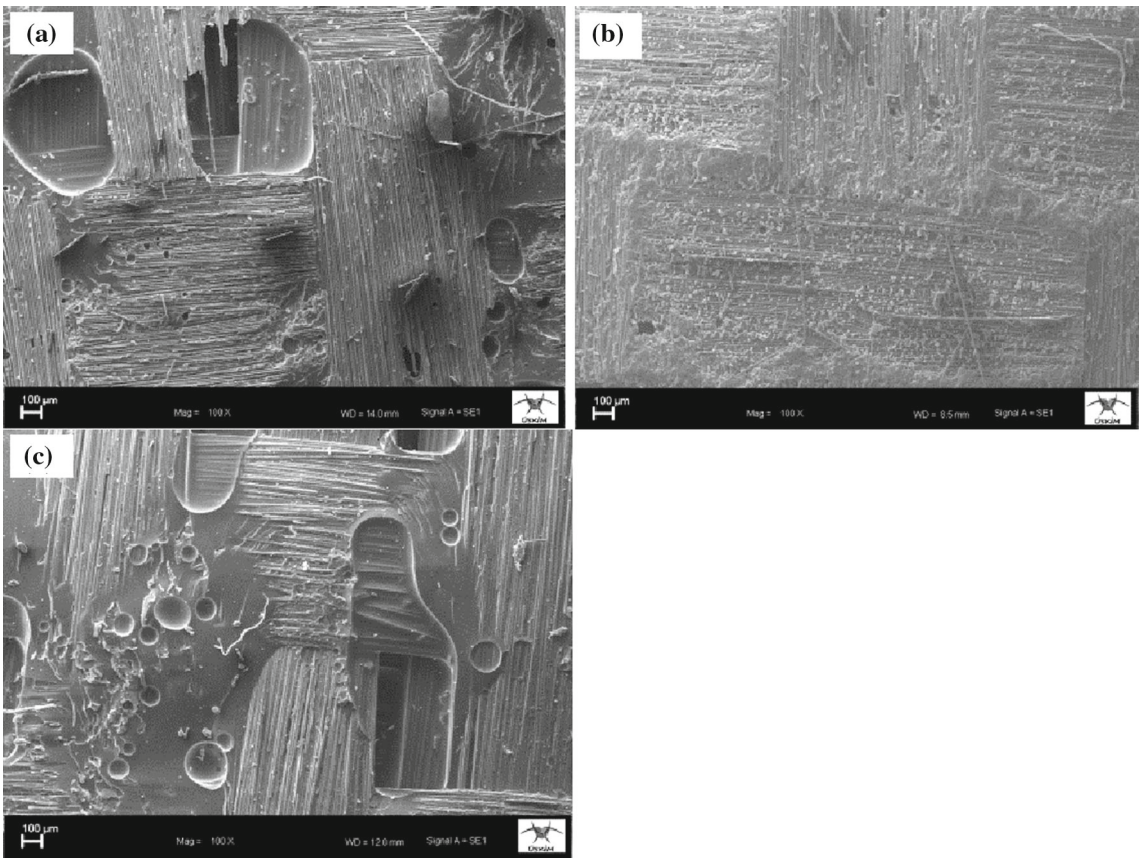

Fig. 8 SEM images of mode I interlaminar fracture surface for: **a** GFRE, **b** Bx_{15}-GFRE, **c** SiC_{10}-GFRE composites

tively, compared with that of GFRE composite. While with SiC addition, the highest increment of G_{IC}-Prop was 27.3% at SiC content of 10 wt%. These slight drops in G_{IC}-Prop values can be described to the negative effects of void content and particle aggregation on the adhesion strength between Bx and SiC particles and matrix, in which they act as stress concentration points and weakened the composite [13,23,39].

3.3 Mechanisms of Mode I Delamination Energy

The fracture surface of DCB specimens was observed using SEM micrographs in order to explain the above mode I interlaminar fracture results for GFRE, Bx-GFRE and SiC-GFRE composites (Fig. 8). The SEM image of the GFRE specimen fracture surface showed the glass fibers pulled out from

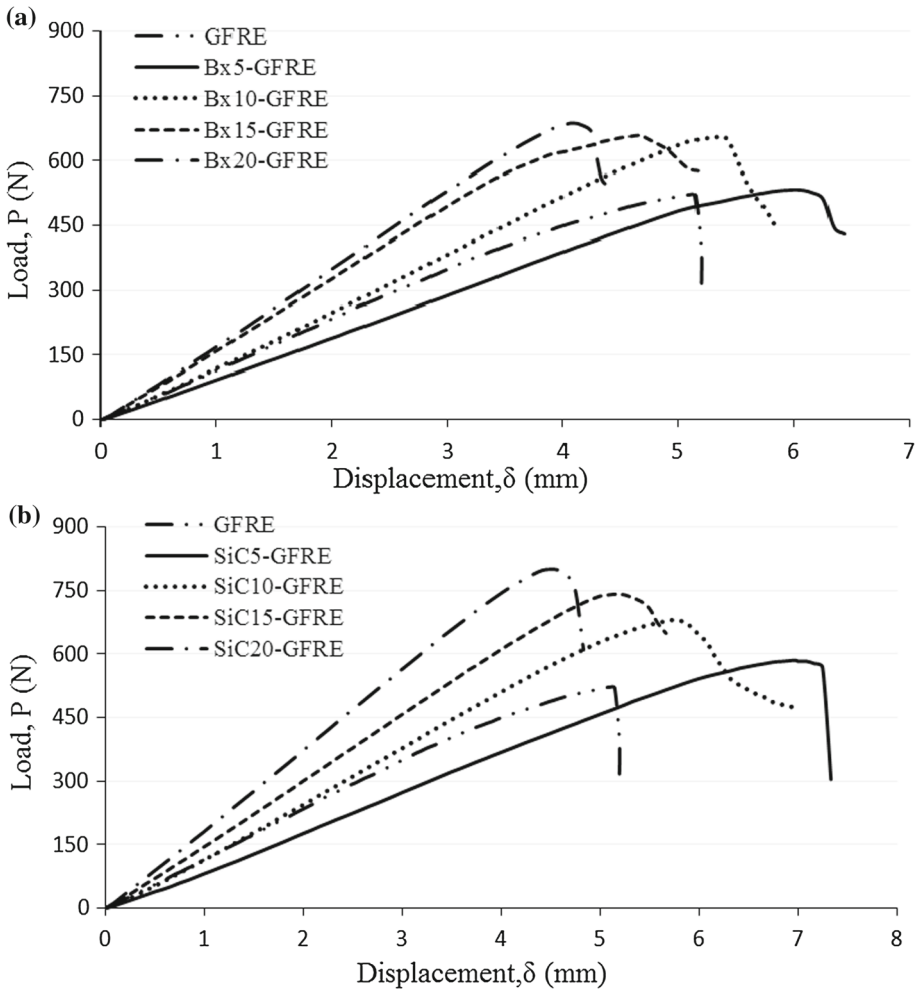

Fig. 9 Load–displacement curves of the ENF tests for the **a** Bx-GFRE and **b** SiC-GFRE composites

matrix (Fig. 8a). On the other hand, for Bx_{15}-GFRE and SiC_{10}-GFRE composites, Bx and SiC particles bonded with matrix and settled around the glass fibers (Fig. 8b, c), these SEM images were taken for the specimens of higher toughness at Bx and SiC content of 15 and 10 wt%, respectively. As shown in SEM images, the crack propagated through the Bx and SiC particles without debonding between particles and epoxy matrix. This proves the chemical compatibility of Bx/epoxy and SiC/epoxy systems. Furthermore, the good adhesion of particle/matrix system was decreased the interlayer region and delayed the plastic zone formation. Hence, the mode I fracture toughness reached highest value when the Bx and SiC contents were 15 and 10 wt% and then followed the trend of decreasing due to particle aggregation, which caused debilitated the adhesion strength between epoxy matrix and particle.

3.4 Effect of Particle Content on Mode II Delamination Energy

The typical load–displacement curves obtained from ENF tests are shown in Fig. 9. The GFRE, Bx-GFRE and SiC-GFRE specimens presented a linear load–displacement behavior up to the point of crack initiation, then load dropped and lead to the unstable crack propagation and fracture. This performance was influenced by brittleness of the epoxy matrix. Furthermore, there was a plateau at the highest load. Therefore, the crack propagation was delayed by inclusion of rigid Bx and SiC particles within GFRE composite [23,34]. The highest load–displacement value of GFRE composite was about 522 N–5.08 mm. Hence, the highest load–displacement was improved with the addition of borax. Hence, the highest load–displacement values of Bx-GFRE composites were 534 N–6.0 mm, 656 N–5.4 mm, 659 N–4.7 mm and 688 N–4.1 mm for borax contents of 5, 10, 15 to 20 wt%, respectively (Table 3). The displacement corresponding to the highest load reduced from 4.67 to 4.08 mm with the borax content increased from 15 to 20 wt%. Same behavior was noticed for SiC-GFRE specimens under ENF test, but the highest mode II toughness occurred at SiC content of 5 wt%.

The highest values of G_{IIC} were 2192 J/m^2 and 2528 at Bx and SiC contents of 10 and 5 wt%, respectively (Fig. 10); then, G_{IIC} reduced gradually for both fillers. Compared with

Table 3 Mode II delamination properties of the composites

Composite type	Borax content (wt%)	Highest load (N)	Displacement at highest load (mm)	Fracture toughness G_{IIC} (J/m^2)	G_{IIC} increment (%)
GFRE	0	522 (±22)	5.08 (±0.12)	1720 (±66)	–
Bx_5-GFRE	5	534 (±11)	5.97 (±0.08)	1996 (±32)	16.0
Bx_{10}-GFRE	10	656 (±09)	5.36 (±0.17)	2192 (±51)	27.6
Bx_{15}-GFRE	15	659 (±13)	4.67 (±0.14)	1921 (±39)	11.6
Bx_{20}-GFRE	20	688 (±15)	4.08 (±0.11)	1749 (±37)	1.7
SiC_5-GFRE	5	585 (±25)	6.97 (±0.13)	2528 (±70)	46.5
SiC_{10}-GFRE	10	681 (±11)	5.76 (±0.04)	2385 (±38)	38.3
SiC_{15}-GFRE	15	742 (±15)	5.16 (±0.12)	2359 (±31)	37.2
SiC_{20}-GFRE	20	800 (±18)	4.50 (±0.09)	2200 (±53)	27.8

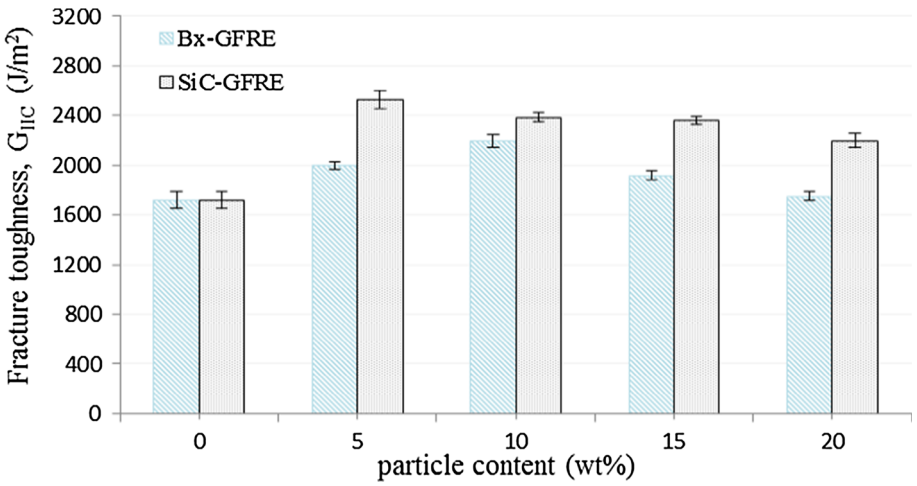

Fig. 10 Comparison of mode II fracture toughness among GFRE, Bx-GFRE and SiC-GFRE composites

that of GFRE composite, G_{IIC} of the Bx-GFRE increased by 16.0, 27.6, 11.6 and 1.7%, respectively, while the highest increment of G_{IIC} for SiC-GFRE composite increased by 46.5%, compared to unfiled GFRE composite.

3.5 Mechanisms of Mode II Delamination Energy

To clarify the mode II delamination results, SEM images were taken for the fracture surface of ENF specimens. Hence, the ENF specimens of GFRE, Bx-GFRE and SiC-GFRE composites were applied to mode II shear loading lead to crack growth through specimen from the crack tip (film insert) to mid-span of the specimen. The mode II fracture of the composites was brittle fracture. Thus, the SEM image of the fracture surface of GFRE specimen showed that the glass fibers were exposed during crack propagation (Fig. 11a). On the other hand, the fracture surface was different after the addition of particles within GFRE composites. Hence, the crack propagated through the Bx and SiC particles without initiating particle/matrix debonding. Moreover, the fracture surface contains hackles that provided more toughening [2,41]. Therefore, the fracture surfaces near the mid-span of the Bx-GFRE and SiC-GFRE composites (Fig. 11b, c) illustrated the plastically deformed zones keep good adhesion among particle/fiber/epoxy system. Chai [42,43] introduced similar concept about the plastic shear deformation as a main parameter effect on the mode II interlaminar toughness. The mode II delamination energy decreased when the Bx and SiC contents were more than 10 and 5 wt%, because of the particle aggregation.

4 Conclusions

The composite laminates of Bx/glass/epoxy and SiC/glass/epoxy were manufactured with Bx and SiC particle content of 0, 5, 10, 15 and 20 wt%. The mechanical properties, DCB and ENF tests were conducted on the composite specimens according to ASTM standards. The main conclusions of this study can be given as:

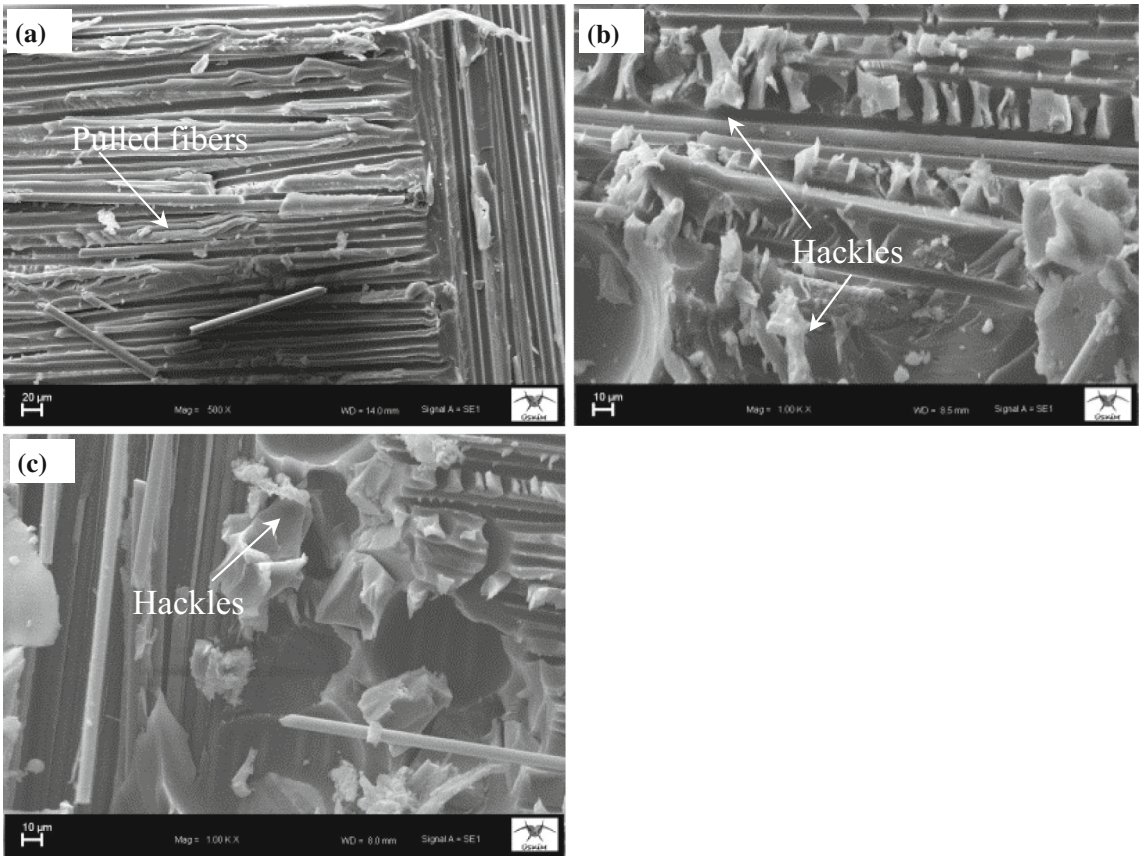

Fig. 11 SEM images of mode II interlaminar fracture surface for: **a** GFRE, **b** Bx_{10}-GFRE, **c** SiC_5-GFRE composites

- The inclusion of Bx and SiC fillers to GFRE composite strongly affected the mechanical properties and delamination energy of mode I and mode II.
- The tensile strength, flexural strength and flexural modulus reached highest values at borax content of 10 wt% with highest increment of 10.5, 51.0 and 16.7%, respectively. These results were better than that of SiC-GFRE composites.
- The optimum values of initiation and propagation of mode I delamination energy, G_{IC}-Onset and G_{IC}-Prop were improved by 45.8 and 33.8%, respectively, at borax content of 15 wt%. On the other hand, G_{IC}-Onset and G_{IC}-Prop were improved by 36.7 and 27.3%, respectively, at SiC content of 10 wt%.
- The values of mode II delamination energy, G_{IIC}, were optimum at Bx and SiC content of 10 and 5 wt%, with highest increment of 27.6 and 46.5%, respectively.
- SEM images showed that the fracture surface was different after the addition of particles that the improvement of mode I and mode II delamination energy related to the high debonding resistance of the Bx and SiC particles from epoxy matrix, and thus, crack growth delayed through specimens during the tests. This mechanism indicates the chemical compatibility of the Bx and SiC particles within GFRE composite.

References

1. Sathishkumar, T.P.; Satheeshkumar, S.; Naveen, J.: Glass fiber-reinforced polymer composites—a review. J. Reinf. Plast. Comput. **33**(13), 1258–1275 (2014)
2. Srivastava, V.K.; Hogg, P.J.: Damage performance of particles filled quasi-isotropic glass-fibre reinforced polyester resin composites. J. Mater. Sci. **33**, 1119–1128 (1998)
3. Salpekar, S.A.; Raju, I.S.; O'Brien, T.K.: Strain-energy-release rate analysis of delamination in a tapered laminate subjected to tension load. J. Compos. Mater. **25**(2), 118–141 (1991)
4. Song, M.C.; Sankar, B.V.; Subhash, G.; Yen, C.F.: Analysis of mode I delamination of zpinned composites using a non-dimensional analytical model. Compos. Part B **43**, 1776–1784 (2012)
5. Mouritz, A.P.; Koh, T.M.: Re-evaluation of mode I bridging traction modeling for z-pinned laminates based on experimental analysis. Compos. Part B **56**, 797–807 (2014)
6. Pegorin, F.; Pingkarawat, K.; Daynes, S.; Mouritz, A.P.: Influence of z-pin length on the delamination fracture toughness and fatigue resistance of pinned composites. Compos. Part B **78**, 298–307 (2015)
7. Mouritz, A.P.; Cox, B.N.A.: mechanistic approach to the properties of stitched laminates. Compos. Part A **31**, 1–27 (2000)

8. Mezzenga, R.; Boogh, L.; Månson, J.-A.E.: A review of dendritic hyperbranched polymer as modifiers in epoxy composites. Compos. Sci. Technol. **61**, 787–795 (2001)
9. Van der Heijden, S.; Daelemans, L.; De Schoenmaker, B.; De Baere, L.; Rachier, H.; Van Paepegem, W.: interlaminar toughening of resin transfer moulded glass fibre epoxy laminates by polycaprolactone electrospun nanofibres. Compos. Sci. Technol. **104**, 66–73 (2014)
10. Dadfar, M.R.; Ghadami, F.: Effect of rubber modification on fracture toughness properties of glass reinforced hot cured epoxy composites. Mater. Des. **47**, 16–20 (2013)
11. Tang, Y.H.; Ye, L.; Zhang, D.H.; Deng, S.Q.: Characterization of transverse tensile, interlaminar shear and interlaminate fracture in CF/EP laminates with 10 wt% and 20 wt% silica nanoparticles in matrix resins. Compos. Part A **42**, 1943–1950 (2011)
12. Fan, Z.; Santare, M.H.; Advani, S.G.: Interlaminar shear strength of glass fiber reinforced epoxy composites enhanced with multi-walled carbon nanotubes. Compos. Part A **39**, 540–554 (2008)
13. Zhu, J.; Imam, A.; Crane, R.; Lozano, K.; Khabashesku, V.N.; Barrera, E.V.: Processing a glass fiber reinforced vinyl ester composite with nanotube enhancement of interlaminar shear strength. Compos. Sci. Technol. **67**, 1509–1517 (2007)
14. Wang, K.; Cheng, L.; Wu, J.S.; Toh, M.L.; He, C.B.; Yee, A.F.: Epoxy Nanocomposites with highly exfoliated clay: mechanical properties and fracture mechanisms. Macromolecules Macromolecules **38**, 788–800 (2005)
15. Coleman, J.N.; Khan, U.; Blau, W.J.; Gun'ko, Y.K.: Small but strong: a review of the mechanical properties of carbon nano tube polymer composites. Carbon **44**, 1624–1652 (2006)
16. Shahid, N.; Villate, R.G.; Barron, A.R.: Chemically functionalized alumina nanoparticle effect on carbon fiber/epoxy composites. Compos. Sci. Technol. **65**, 2250–2258 (2006)
17. Gardea, F.; Lagoudas, D.C.: Characterization of electrical and thermal properties of carbon nanotube/epoxy composites. Compos. Part B **56**, 611–620 (2014)
18. Jiang, Q.; Wang, X.; Zhu, Y.; Hui, D.; Qiu, Y.: Mechanical, electrical and thermal properties of aligned carbon nanotube/polyimide composites. Compos. Part B **56**, 408–412 (2014)
19. Shiu, S.-C.; Tsai, J.-L.: Characterizing thermal and mechanical properties of graphene/epoxy nanocomposites. Compos. Part B **56**, 691–697 (2014)
20. Chen, Q.; Wu, W.; Zhao, Y.; Xi, M.; Xu, T.; Fong, H.: Nano-epoxy resins containing electrospun carbon nanofibers and the resulting hybrid multi-scale composites. Compos. Part B **58**, 43–53 (2014)
21. Hsieh, T.H.; Huang, Y.S.: The mechanical properties and delamination of carbon fiber-reinforced polymer laminates modified with carbon aerogel. J. Mater. Sci. **52**, 3520–3534 (2017)
22. Wang, Z.; Huang, X.; Bai, L.; Du, R.; Liu, Y.; Zhang, Y.; Zaho, G.: Effect of micro-Al_2O_3 contents on mechanical property of carbon fiber reinforced epoxy matrix composites. Compos. Part B **91**, 392–398 (2016)
23. Chisholm, N.; Mahfuz, H.; Rangari, V.K.; Ashfaq, A.; Jeelani, S.: A comparative study on different ceramic fillers affecting mechanical properties of glass-polyester composites. Compos. Struct. **67**, 115–124 (2005)
24. U.S. Borax Inc. Material Safety Data Sheet DATE OF ISSUE. Occupational Health & Product Safety Department, pp. 1–4 (2000)
25. Boncukcuoglu, R.; Yilmaz, M.T.; Kocakerïm, M.M.; Tosunoglu, V.: Utilization of trommel sieve waste as an additive in Portland cement production. Cem. Concr. Res. **32**, 35–39 (2002)
26. Mouritz, A.P.; Gibson, A.G.: Fire Properties of Polymer Composite Materials, p. 385. Springer, Berlin (2006)
27. Shen, K.K.; Kochesfahani, S.H.; Jouffret, F.: Boron-Based Flame Retardants and Flame Retardancy. CRC Press, Boca Raton (2010)
28. Cavdar, A.D.; Mengeloglu, F.; Karakus, K.: Effect of boric acid and borax on mechanical, fire and thermal properties of wood flour filled high density polyethylene composites. Measurement **60**, 6–12 (2015)
29. Ayrilmis, N.; Akbulut, T.; Dundar, T.; Robert, H.W.; Mengeloglu, F.; Buyuksari, U.; Candan, Z.; Avci, E.: Effect of boron and phosphate compounds on physical, mechanical, and fire properties of wood-polypropylene composites. Constr. Build. Mater. **33**, 1263–1269 (2012)
30. Gumus, O.Y.; Erol, Y.; Unal, H.I.: Polythiophene/borax conducting composite II: electrorheology and industrial applications. Polym. Compos. **10**, 756–765 (2011)
31. ASTM Standard D 5528-94a. Test Method for Mode I Interlaminar Fracture Toughness of Unidirectional Fiber-Reinforced Polymer Matrix Composites, American Society for Testing and Materials, West Conshohocken, PA (2001)
32. Almansour, F.A.; Dhakal, H.N.; Zhang, Z.Y.: Effect of water absorption on Mode I interlaminar fracture toughness of flax/basalt reinforced vinyl ester hybrid composites. Compos. Struct. **168**, 813–825 (2017)
33. Albertsen, H.; Ivens, J.; Peters, P.; Wevers, M.; Verpoest, I.: Interlaminar fracture toughness of CFRP influenced by fiber surface treatment: part 1 experimental results. Compos. Sci. Technol. **54**, 133–145 (1995)
34. Seyhan, A.; Tanoglu, M.; Schulte, K.: Mode I and mode II fracture toughness of E-glass non-crimp fabric/carbon nanotube (CNT) modified polymer based composites. Eng. Fract. Mech. **75**, 5151–5162 (2008)
35. Dharmawan, F.; Simpson, G.; Herszberg, I.; John, S.: Mixed mode fracture toughness of GFRP composites. Comps. Struct. **75**, 328–338 (2006)
36. Carlsson, L.A.; Gillespie, J.W.; Pipes, R.B.: On the analysis and design of the end notched flexure (ENF) specimen for Model II testing. J. Compos. Mater. **20**, 594–604 (1986)
37. Lee, J.J.; Lim, J.O.; Huh, J.S.: Mode II interlaminar fracture behavior of carbon bead-filled epoxy/glass fiber hybrid composite. Polym. Compos. **21**, 343–352 (2000)
38. Srivastava, V.K.; Hogg, P.J.: Moisture effects on the toughness, mode-I and mode-II of particles filled quasi-isotropic glass-fiber reinforced polyester resin composites. J. Mater. Sci. **33**, 1129–1136 (1998)
39. Lee, S.M.: Mode II delamination failure mechanisms of polymer matrix composites. J. Mater. Sci. **32**, 1287–1295 (1997)
40. Wang, T.W.; Daharani, L.R.: Effect of interfacial mobility on flexural strength and fracture toughness of glass/epoxy laminates. J. Mater. Sci. **34**, 4873–4882 (1999)
41. Stevanovic, D.; Kalyanasundaram, S.; Lowe, A.; Jar, P.-Y.B.: Mode I and mode II delamination properties of glass/vinyl-ester composite toughened by particulate modified interlayers. Compos. Sci. Technol. **63**, 1949–1964 (2003)
42. Chai, H.: Observation of deformation and damage at the tip of cracks in adhesive bonds in shear and assessment of a criterion for fracture. Int. J. Fract. **60**, 311–326 (1993)
43. Chai, H.: Micromechanics of shear deformation in cracked bonded joints. Int. J. Fract. **58**, 223–239 (1992)